C h a p t e r VIII

All Grown Up: Leaving the Nest

> Your children are not your children. They are the sons and daughters of Life's longing for itself. They come through you but not from you, And though they are with you yet they belong not to you. You may give them your love but not your thoughts, For they have their own thoughts. You may house their bodies but not their souls, For their souls dwell in the house of tomorrow, which you cannot visit, not even in your dreams. You may strive to be like them, but seek not to make them like you. For life goes not backward nor tarries with yesterday.
>
> Kahlil Gibran, *The Prophet*

"She's Leaving Home"

by John Lennon / Paul McCartney

The idea to explore the rate of elongation of bubbles was suggested with guidance by Prof. Howard Stone of Princeton University, NJ. Thanks to Profs. John Brady and Richard Flagan for helpful discussions.

Bubbles do not remain solitary and spherical forever. As they grow, they eventually come in contact with their environment, deforming upon brushing up against other bubbles and reaching the limits of their confinement. At this point, it

is time to get out. As bubbles deform under confinement, they also accelerate to the outlet, as if more fervently seeking escape. Others may find themselves squeezed against other bubbles along the way. The confinement may cause them to merge into one.

Typically, in the flow-focusing channel presented in Chapter III, bubbles first deform upon growing to the size of the diameter of the inner stream due to the higher viscosity of the outer stream than the inner. When bubbles span the width of the inner stream, additional interactions emerge, such as the formation of a "wake" with a different index of refraction behind the bubble (Section VIII.2). These differences in the index of refraction are caused by differences in CO_2 concentration, which affects where bubbles nucleate in the wake. As is often the case following such nucleation events in the wake, bubbles are squeezed against each other. In this case, coalescence is too slow to allow them to merge: ripening is the faster merging process (Section VIII.3). When enough bubbles have nucleated and grown large enough, the inner stream viscosity decreases significantly, which can lead to instabilities (Section VIII.4). While these instabilities preclude observation of bubble nucleation and growth, they are fascinating to watch and important to understand to determine the parameter ranges in which our flow-focusing method can be operated.

VIII.1 Bubbles Elongate Upon Facing Viscous Resistance from Outer Stream

Upon reaching the interface between between the inner and outer streams, bubbles face significant viscous resistance from the outer stream (viscosity almost 5 Pa.s; see Figure III.S1). The viscosity of the inner stream may be as low as 0.01 Pa.s, however, so the bubble can grow much more easily along the flow axis than radially into the outer stream. Consequently, the bubble elongates along the flow direction as if flowing inside a rigid tube rather than confined by a high-viscosity sheath, as shown in Figure VIII.1. The wake that the bubble later leaves behind as it elongates is discussed in the following Section (Section VIII.2).

Bubbles Elongate Exponentially in Time

The models of bubble growth presented in Chapter V no longer describe the growth of a bubble accurately after it reaches the surface of the inner stream and begins to elongate. At this point, the width of the bubble along the radial direction of the capillary remains roughly fixed at the width of the inner stream. The length of the bubble along the flow axis grows exponentially. The square-root growth characteristic of an isolated, spherical bubble and the exponential elongation of the

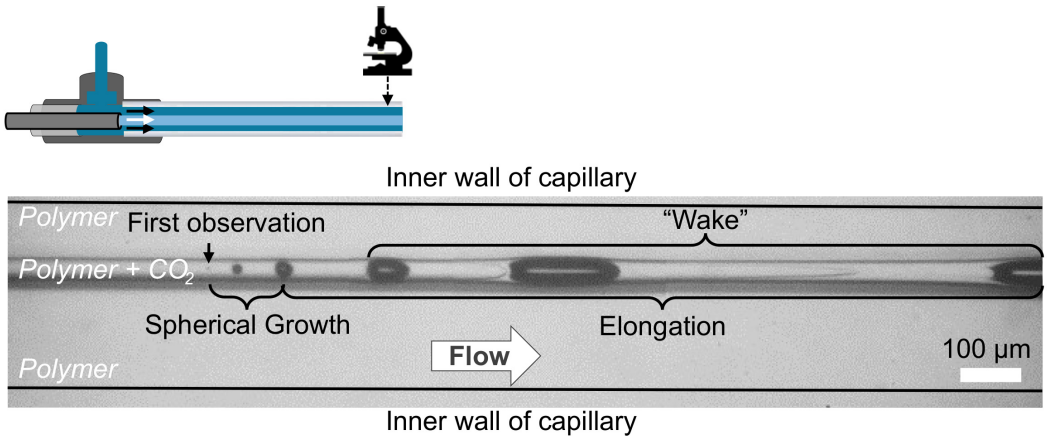

Figure VIII.1: Experimental conditions: PPG 2700 g/mol saturated with CO_2 at 7.0 MPa and 22 °C is flowed through a sheath of 1k5f polyol (see Table II.1) inside a quartz observation capillary with inner diameter 300 μm, length 100 mm, and inlet pressure of about 9.5 MPa, observed 94 mm along the observation capillary. Snapshots of a single bubble from first observation to exit from the field of view are superimposed to show the stages of bubble growth. Initially, the bubble grows spherically. Upon reaching the surface of the inner stream, the bubble elongates along the flow direction. During this elongation, the convection of fluid from the head to the tail of the bubble creates a "wake" behind the bubble (discussed in Section VIII.2). Location of measurement along observation capillary is shown schematically above figure.

bubble under confinement can be seen in the plots of bubble length L (distance from the head to the tail of the bubble), bubble diameter D (width along the radial dimension), and diameter of an equivalent sphere $D_{eq} = \left(\frac{6}{\pi}V\right)^{1/3}$ (where $V = \pi/6D^2L$ is the approximate volume of the bubble assuming an elliptical shape) in Figure VIII.2. The qualitative change in the growth rate can be seen in the linear plot in panel (a). Panel (b) plots the size along a logarithmic vertical axis, such that exponential growth appears as a straight line. Indeed, the growth of the length of the bubble L (blue line) matches the straight line shown for reference after the length exceeds the maximum diameter around 500 μs, indicating exponential growth. In this case, the time constant corresponding to the straight line is about 1 ms, meaning that the bubble grows by a factor of e every millisecond. Panel (c) plots both axes on a logarithmic scale, such that a power-law growth appears as a straight line with the power equal to the slope. Indeed, the growth of the bubble diameter D (orange line) grows with a power of 1/2, consistent with the observations in Chapter V. While the diameter of an equivalent sphere D_{eq}—an estimate of the diameter of the bubble if it were growing unhindered—appears in panel (c) to grow with a power

of 1/2 as well, even after the bubble has started elongating, the growth should be exponential since it is proportional to the cube root of the length. We suspect that this coincidence is the result of only observing a short segment of the exponential growth regime, which may look linear with a slope of 1/2 on a log-log scale for this brief period of time.

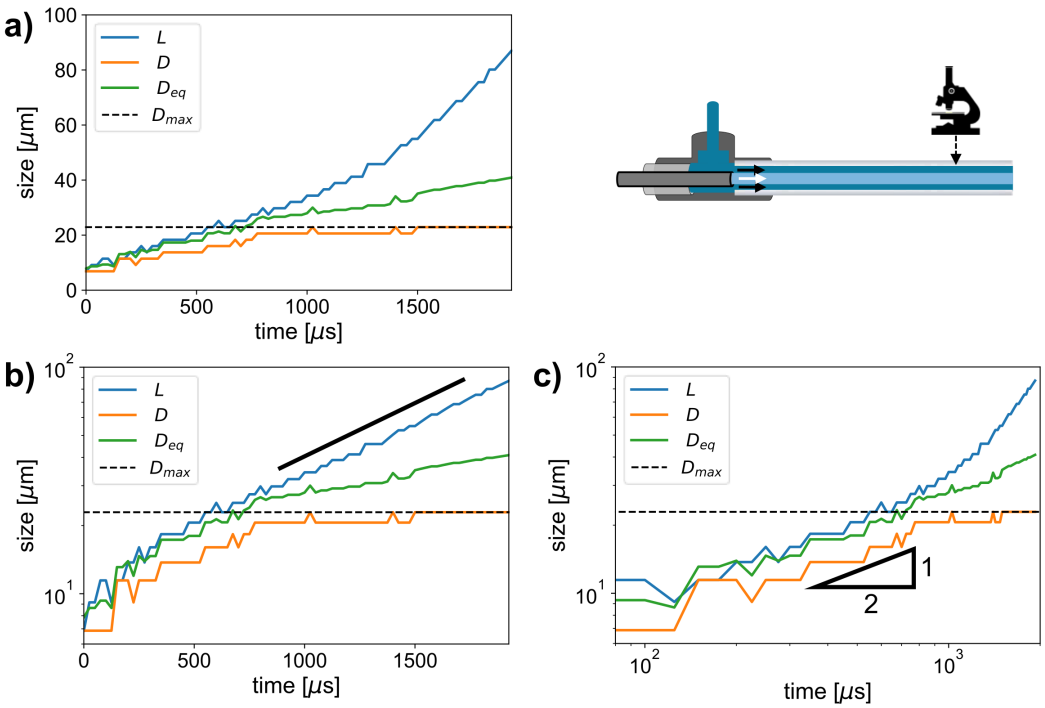

Figure VIII.2: A bubble's length L from head to tail (blue line), diameter D along the radial direction (orange line), equivalent diameter of a sphere of the same volume $D_{eq} = (D^2 L)^{1/3}$ (green line), and maximum diameter of the bubble (black dashed line) are plotted as a function of time. a) Linear scale for both axes. b) Logarithmic vertical scale. Black line provided as a reference to represent exponential growth with a growth constant of about 1 ms. c) Logarithmic vertical and horizontal axes. A slope of 1/2 is indicated by the triangle, which represents power-law growth $t^{1/2}$. The bubble analyzed comes from an observation taken during the experiment as in Figure VIII.1 but at 79 mm downstream.

The exponential elongation of bubbles under confinement has been observed before in the case of a vapor bubble in a boiling liquid flowing through a tube [1–3]. Exponential growth results from a growth rate of a dimension proportional to the size of that dimension. In this case, it suggests that $\frac{dL}{dt} \propto L$. Such growth is consistent with a flux that is constant when averaged along the length of the bubble, suggesting that CO_2 is not depleted significantly in the region immediately surrounding an elongated bubble, as if it is replenished. We explore this idea of replenishing CO_2

around elongated bubbles in Section VIII.2.

Bubbles Accelerate as They Elongate Due to Fluid Displaced by Growth

When a bubble elongates, it does so because it cannot push fluid around its lateral sides out of the way. Instead, fluid must be displaced at the head or tail of the bubble to permit the growth, assuming it is flowing in an incompressible fluid medium. Where does the fluid displaced by the elongation of the bubble go? While we cannot observe the flow field directly, nor can we place tracer particles into the inner stream because they would cause heterogeneous bubble nucleation, we can occasionally observe the flow indirectly by watching small bubbles.

In Figure VIII.3, we show that three small bubbles remain almost perfectly still as an elongated bubble passes by them. Two of the three bubbles can be seen in front of the elongated bubble in panel (a) (circled in yellow). The locations of the three bubbles are marked by yellow circles in three frames as the elongated bubble passes by them over the course of 440 μs (panels b–d). The right most edge of the marker circles in panel (d) is marked with a thin vertical yellow line to provide a guide to the eye for comparing the positions of the bubbles. Over the last 240 μs, the small bubbles translate less than 5 % of the distance traveled in the first 200 μs of the sequence of frames. This near-stagnation of the bubbles within the thin film between the bubble and the outer stream reveals that fluid at the head of the bubble ends up at the tail of the bubble as the bubble "slips past" the fluid. While in the laboratory frame of reference, the fluid in this film moves little, relative to the flow upstream and downstream, the fluid is moving upstream. A similar stagnation is observed in the outer stream, as shown in Figure VIII.S1 of the Supporting Information (SI).

Agostini *et al.* suggest that the fluid in the thin film between the bubble and the confining surface appears to flow upstream relative to the flow because it is the path of least resistance for fluid displaced by the growing bubble [2]. A schematic showing this process is presented in Figure VIII.4. In panel (a), at time t_i, a volume ΔV_b^i of the inner stream fluid surrounds the head of the bubble. This volume is equal to the volume by which the bubble will grow in a time step Δt, as shown in green in panel (b). The displaced fluid has nowhere to go but upstream to the tail of the bubble, as shown in panel (c), during which the fluid faces little resistance from the pressure upstream because the pressure along a bubble is negligible (see Figure 8 of Khandekar *et al.* [4]). Assuming that the bubble is incompressible, the fluid displaces the bubble, pushing the bubble farther downstream, as shown in panel (d).

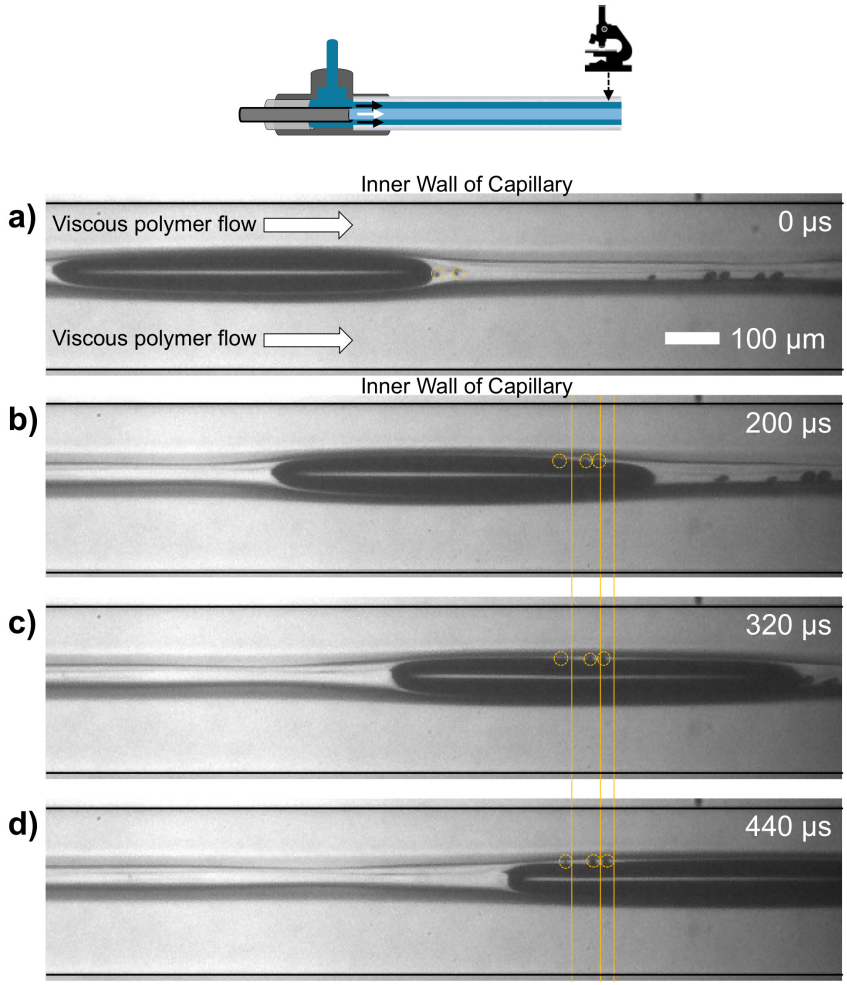

Figure VIII.3: a-d) Still frames of sheath flow show small bubbles stagnate in the thin film between an elongated bubble and the outer stream as the elongated bubble passes by them. Yellow dashed circles mark three small bubbles that act as tracers of the flow (one of these bubbles is not visible in (a)). The far-right edge of these circles in the final frame (d) is marked by vertical yellow lines. In the 240 μs between (b) and (d), the bubbles hardly move a few μm while they travel hundreds of μm in the 200 μs between (a) and (b). Top shows a schematic of where the observation was made along the observation capillary. PPG 2700 g/mol polyol (see Table II.1) saturated with CO_2 at 7.2 MPa and 22 °C flowed within sheath of 1k5f polyol in a quartz observation capillary of 300 μm inner diameter and 100 mm length with an inlet pressure of 13.4 MPa and observed at 95 mm along the length of the capillary.

During the time step Δt, the surrounding fluid has been flowing at a speed U_l and thus has traveled a distance $U_l \Delta t$, as shown in panel (e). Consequently, over a time step Δt, the bubble travels farther than the surrounding fluid medium.

This circulation of flow causes bubbles growing in confinement to accelerate with their length [1, 2]. We show this acceleration in Figure VIII.5. In panel (a), we

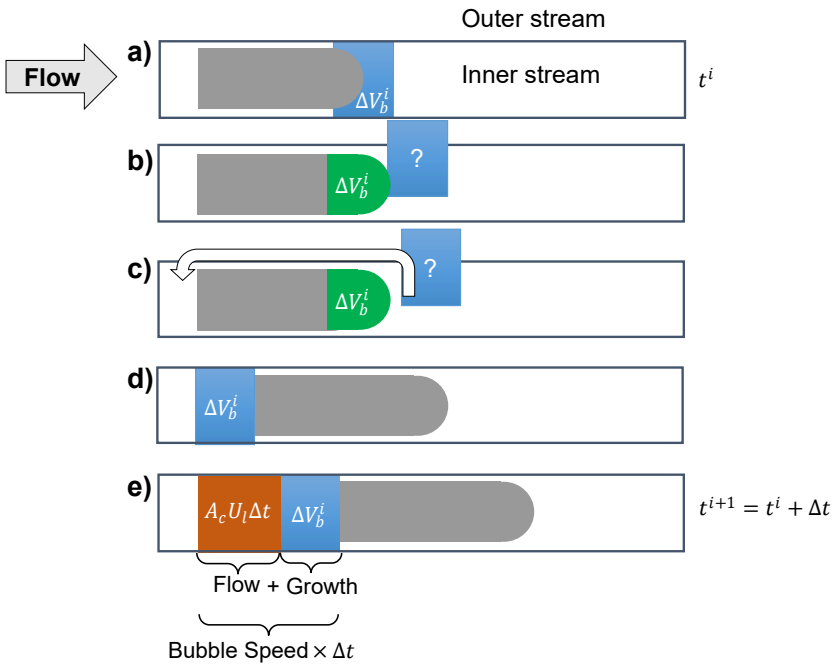

Figure VIII.4: Schematic showing that the displacement of fluid by an elongating bubble under confinement causes the bubble to accelerate faster than the surrounding medium. The black rectangle represents a segment of the inner stream; the area outside it represents the outer stream. Flow is left to right. a) At time t^i, a volume of fluid ΔV_b^i (blue) surrounds the head of the bubble (gray). b) The bubble grows by a volume ΔV_b^i (green) during the timestep Δt and the fluid around it must be displaced somewhere. c) The displaced fluid (blue) can only flow upstream to the tail of the bubble. d) Upon reaching the tail of the bubble, the displaced fluid (blue) displaces the bubble (gray) farther downstream. e) During the timestep Δt, the flow also travels a distance $U_l \Delta t$ (orange) which, when combined with the distance the bubble is displaced by the displaced fluid, results in the distance traveled by the bubble. The resulting bubble speed is larger than the flow speed.

plot the speed of the head (yellow) and tail (blue) of a large collection of bubbles observed at 88 mm and 90 mm along the length of the observation capillary. The data were collected from the same experiment as was used to estimate the rate of bubble nucleation in mixtures of PPG and CO_2 in Section VI.2: the inner stream is composed of PPG 2700 g/mol saturated with CO_2 at 7.2 MPa and 22 °C and the outer stream is composed of 1k5f polyol (see Table II.1), flowing through a capillary with an inner diameter of 300 μm and a length of 100 mm with an inlet pressure of 13.4 MPa. While the data do not perfectly collapse, some general trends are observed. When the bubble is smaller than the inner stream, the speed appears to decrease with length, possibly because the flow nearer the surface of the inner stream is slower. Once the bubble is longer than the width of the inner stream,

meaning that it is flowing under confinement inside the highly viscous outer stream, the speed increases with length. This increase is roughly linear until the bubble reaches a length of around 400 μm. Above 400 μm, further elongation of the bubble leads to little acceleration of the tail as the speed appears to plateau, while the head accelerates (as must be the case assuming an incompressible system) but less rapidly than for lengths below 400 μm.

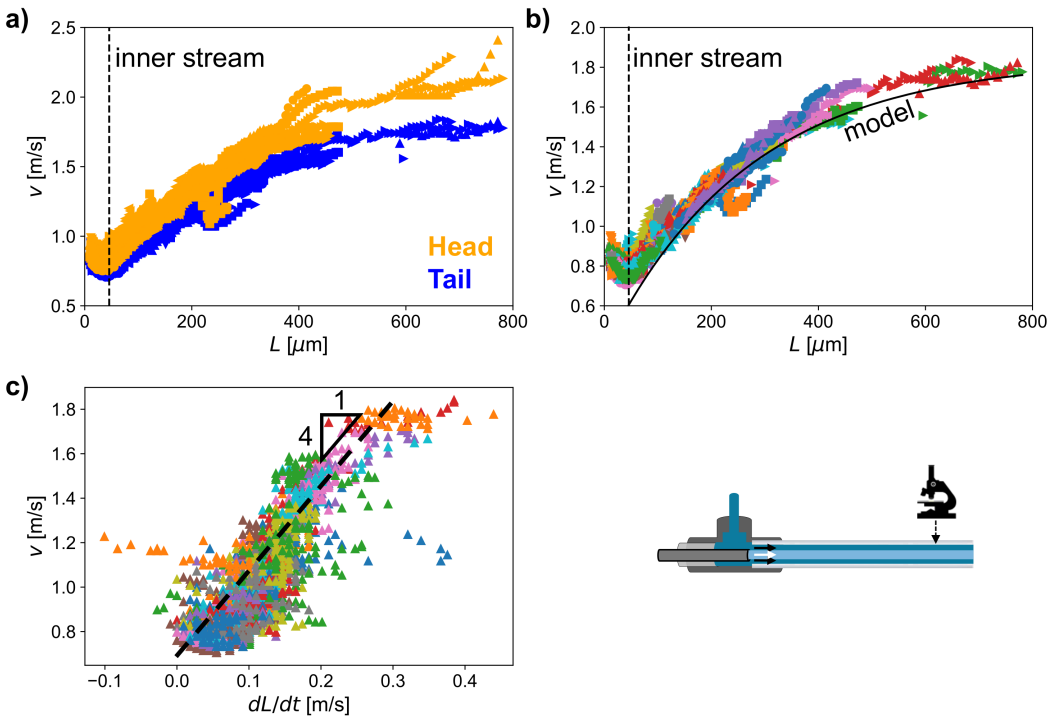

Figure VIII.5: Bubble speed as a function of length and elongation rate. a) The speed of the bubble head (yellow) and tail (blue) as a function of the length of the bubble. The vertical dashed line indicates the width of the inner stream; data points to the right of this line represent elongated bubbles. b) Only the data for the speed of the bubble tail from (a) are shown. Each color and symbol represents a different bubble as it grows. A fitted model based on the work of Agostini et al. [2] is shown (black solid line). c) Speed of the bubble tail as a function of $\mathrm{d}L/\mathrm{d}t$, the rate at which the bubble length L increases. The estimate for $\mathrm{d}L/\mathrm{d}t$ is prone to noise due to limited spatial and time resolution and imperfect image segmentation. A linear fit with a slope of 4 is shown (black dashed line). Lower right indicates schematically where observations were taken along the observation capillary. PPG 2700 g/mol polyol (see Table II.1) saturated with CO_2 at 7.2 MPa and 22 °C flowed within sheath of 1k5f polyol in a quartz observation capillary of 300 μm inner diameter and 100 mm length with an inlet pressure of 13.4 MPa and observed at 95 mm along the length of the capillary.

Out of curiosity, we fit the collection of bubble speeds vs. lengths to a model

proposed by Agostini *et al.* for vapor bubbles flowing through a tube of boiling liquid refrigerant, as shown in Figure VIII.5b. The model assumes that the flux of gas into the bubble is proportional to the surface area of the bubble, that the fluid displaced by the bubble flows to its tail and pushes the bubble farther downstream, that the system is incompressible, and that the bubble feels an empirical friction force from flowing along the walls, which is responsible for causing the speed to plateau with length [2]. While we cannot comment on the validity of the assumption that friction causes the speed to plateau, but the model appears to capture the speed of the tail of the bubble well, suggesting that similar physics might be at play even though the systems are different. The model is least accurate when the bubble is smaller than the inner stream and not confined, indicating that different physics are dominant when a bubble is flow without the effects of confinement.

Out of further curiosity, we tested a hypothesis that the rate at which the bubble elongates is proportional to the speed of the bubble. This hypothesis was based on the assumption that the elongation of a bubble displaces fluid that flows to the tail of the bubble and pushes the bubble farther downstream, as depicted in Figure VIII.4. If this picture were true, the bubble would accelerate more the faster it grew because it would displace more fluid behind it, pushing it farther downstream in the same time period. To test this hypothesis, we plotted the bubble speed v as a function of the elongation rate $\mathrm{d}L/\mathrm{d}t$ in Figure VIII.5c using the same collection of data as used to generate the plots in the other panels of the Figure. While the spread in the data is large, a general increase of speed with the elongation rate is observed having a slope of 4 (dashed black line). Therefore, while the bubble speed generally increases with the elongation rate, it does so at a rate four times faster. This difference in rate suggests that other physics than just the displacement of fluid by bubble growth depicted in Figure VIII.4 might be responsible for the acceleration of the bubble, such as the acceleration of the flow itself due to the decreased viscous resistance of longer bubbles.

VIII.2 Formation of the Wake

That fluid at the head of an elongated bubble ends up at its tail not only results in the acceleration of the bubble, but it also changes the concentration of CO_2 in the region behind the bubble. This change in concentration of CO_2 is seen behind the longer bubbles in Figure VIII.1, where a dark interface with the shape of a backward "C" is observed. An interface indicates a difference in the index of refraction, which could only be caused by a difference in the concentration of

CO_2 since there is no evidence that the outer stream polyol is mixing with the inner stream. We call the region between the tail of the bubble and this interface the bubble's "wake." Because the bubble accelerates as it grows under confinement, as discussed in the previous Section, the length of the wake increases with time, as seen in Figure VIII.1. The interface at the end of the wake also becomes stratified, likely due to the parabolic shape of the flow speed along the width of the inner stream. This interface indicates an inhomogeneous concentration of CO_2, but where is the CO_2 concentration greater and where is it lower? In the following discussion, we present a model of the wake to shed light on the relative CO_2 concentrations throughout it.

Wake's Anatomy

Why is it important to understand the wake's "anatomy"? Long bubbles can leave behind even longer wake regions, which may affect the likelihood that bubbles nucleate in these regions depending on the concentration of CO_2 (the "anatomy") within them. In experiments, we have observed the effects of different concentrations of CO_2 in the wake. For example, a bubble in the wake of another bubble often grows more slowly than the leading bubble. Additionally, we have seen under high contrast (achieved by narrowing the aperture on the condenser lens of the microscope) that the wake contains a narrow "trail" along its center, as seen in Figure VIII.6. Furthermore, when bubbles nucleate in the wake, they tend to nucleate near but outside this trail, as observed in the cluster of recently nucleated bubbles in the lower part of the Figure (outlined in a blue dashed rectangle).

To understand the wake's "anatomy," we begin where the fluid from the wake originates based on the discussion in Section VIII.1: the head of the bubble. We show a schematic of the thin film of the inner stream fluid between the head of an elongated bubble and the outer stream in Figure VIII.7. An example of an elongated bubble from an experiment is shown in the lower right with the region of interest outlined with a dashed white rectangle. We consider the reference frame of the bubble, so the acceleration of the bubble causes the inner stream to appear to be flowing toward the tail of the bubble (to the left in the Figure). As the inner stream "flows" at speed U to the left along the bubble, it is squeezed into a thin film with a width δ of a few microns. This film is significantly smaller than either the radius R or length L of the bubble, so we expand it for clarity (not to scale). The pressure inside the bubble is roughly the local fluid pressure (the Laplace pressure is negligible for bubbles larger than 1 μm as shown in Figure V.7), while the inner stream was saturated with CO_2 at a higher pressure. Thus, the equilibrium concentration of CO_2

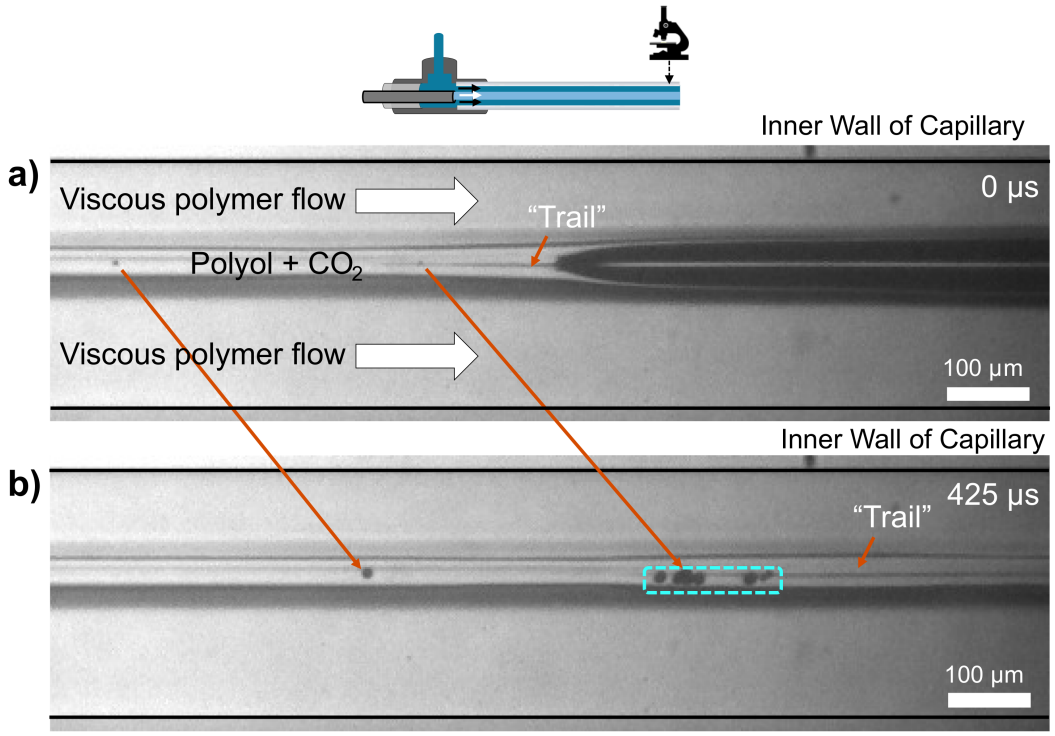

Figure VIII.6: a) Micrograph of the microfluidic sheath flow (location indicated in schematic at top). An elongated bubble is exiting the field of view and leaving behind a "trail" of different index of refraction within the inner stream. b) Micrograph of same location taken 425 μs later. In addition to the bubbles seen in the top image—indicated by orange arrows—many bubbles emerge along the "trail" left behind by the elongated bubble (light blue dashed rectangle). PPG 2700 g/mol polyol (see Table II.1) saturated with CO_2 at 7.2 MPa and 22 °C flowed within sheath of 1k5f polyol in a quartz observation capillary of 300 μm inner diameter and 100 mm length with an inlet pressure of 13.4 MPa and observed at 95 mm along the length of the capillary.

near the surface of the bubble is smaller than the concentration in the inner stream, driving diffusion of CO_2 from the inner stream into the bubble. The front of this diffusion of CO_2 expands into the thin film of the inner stream to have a width that grows as the square root of time since first contact of the fluid with the bubble τ and diffusivity $\mathcal{D}$, $\delta_D \sim \sqrt{\mathcal{D}\tau}$. At the tail of the bubble, the time since contact $\tau = L/U$. The width of the depletion layer at the tail of the bubble is thus $\delta_D \sim \sqrt{\mathcal{D}L/U}$.

Let's estimate the scale of width of this depletion layer. Based on the measurements of diffusivity with G-ADSA shown in Figure II.4, the diffusivity ranges between $\mathcal{D} \in [10^{-10}, 2\times10^{-9}]$ m^2/s. Based on the sample of bubble lengths and speeds plotted in Figure VIII.5, $L \in [50, 800]$ μm and $U \in [0.7, 2.5]$ m/s. Lengths and speeds are correlated, however, so the ratio L/U ranges from 5×10^{-5}

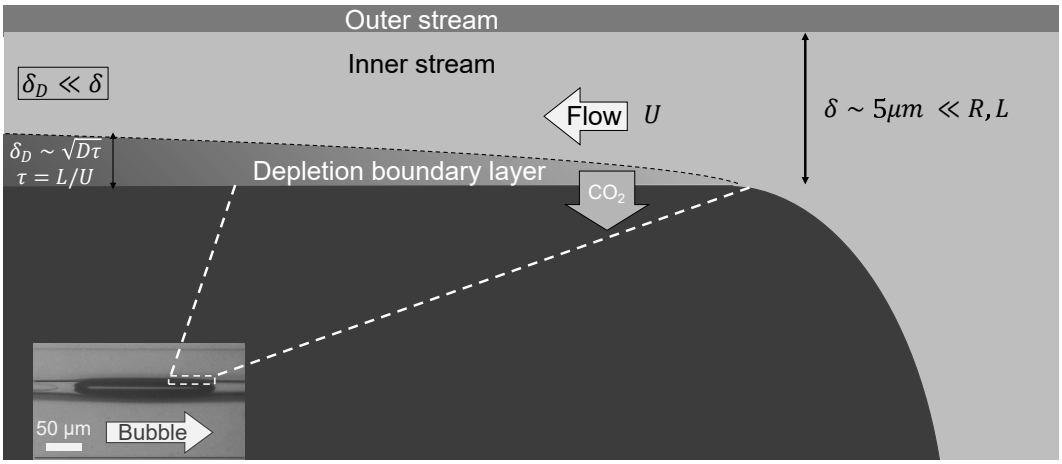

Figure VIII.7: Schematic of the depletion layer along the head of an elongated bubble (location indicated in micrograph in the lower left). The schematic is depicted in the reference frame of the bubble (dark gray region), so the inner stream (light gray region) appears to flow left along the bubble with speed U. The width of the thin film of the inner stream between the bubble and the outer stream (gray region at the top) $\delta \sim 5$ μm, which is much smaller than the radius R or length L of the bubble. As the bubble passes the inner stream, CO_2 diffuses from the inner stream into the bubble, leading to a depletion boundary layer along the bubble (outlined with a dashed black line; darker shade indicates less CO_2). The width of this boundary layer δ_D scales with the square-root of the diffusivity of CO_2 $\mathcal{D}$ and the time for inner stream to pass along the full length of the bubble $\tau = L/U$. Not to scale.

m / 0.7 m/s $\approx 7 \times 10^{-5}$ s (shortest bubbles) to 8×10^{-4} m / 2.5 m/s $\approx 3 \times 10^{-4}$ s (longest bubbles). Therefore, $\delta_D \in [0.1, 0.6]$ μm, meaning that it is significantly thinner than the width of the thin film of inner stream (about 5 μm based on visual observation). Only a small fraction of the thin film nearest the bubble is depleted of CO_2.

How does the fact that the depletion layer along the bubble is much thinner than the film between the bubble and the outer stream affect the fluid in the wake? We show our hypothesis for the concentration of CO_2 in the wake of the bubble as a result of only partial depletion of the thin film along the bubble in Figure VIII.8. As the depletion layer is passed by the tail of the bubble, it is pulled into the center of the inner stream. The remaining volume around it is filled by the rest of the thin film around the bubble. This thin film has another depletion layer along the interface with the outer stream, however, because CO_2 diffuses out from the inner stream of polyol and CO_2 into the pure polyol outer stream. The result of this depletion is depicted by a gradient from dark (low CO_2 concentration) to light (high CO_2 concentration) from the outside to the inner part of the inner stream. The concentration of CO_2 is

thus highest in between these two depletion layers. Therefore, there is a gradient in the concentration of CO_2 along the edge of the depletion.

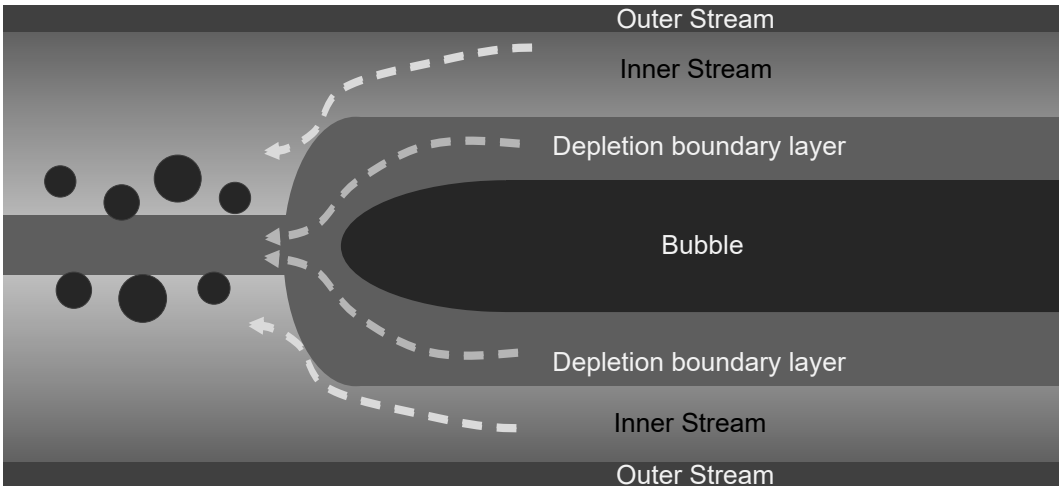

Figure VIII.8: Hypothesis for the explanation of the "trail" observed in Figure VIII.6. The depletion boundary layer at the tail of a bubble (compare with the depletion layer at the head in Figure VIII.7). Because the speed of the bubble scales with its length (see Figure VIII.5), the width of the depletion boundary layer δ_D is less than the width of the inner stream δ (see Figure VIII.7). At the tail of the bubble, the depletion boundary layer fills in the space behind the bubble. Due to the lower concentration of CO_2 (see Figure VIII.9), the index of refraction of the depletion boundary layer is lower than the rest of the inner stream, yielding a visible "trail" behind the bubble (darker gray region). The remainder of the inner stream also loses CO_2 through diffusion into the outer stream (dark gray, top and bottom), yielding a gradient in CO_2 increasing from outside in. This gradient is smoother because it has been formed since the inner and outer streams met at the entrance of the observation capillary. The greatest concentration of CO_2 in the "wake" region behind the elongated bubble is just outside the trail, which may explain why bubbles are often observed to nucleate in this region (see Figures VIII.6 and VIII.S2).

We hypothesize that this concentration gradient leads to a sufficient gradient in the index of refraction that an interface can be distinguished along it, which may be the interface observed along the "trail" observed in the wake (Figure VIII.6). The cause for the sharpness of the interface is not clear, however. Because bubble nucleation is highly sensitive to the degree of supersaturation, it is most likely to occur in the region of highest CO_2 concentration. Based on our hypothetical model, this region lies just outside the depleted trail at the center of the wake, consistent with the observation of bubble nucleation in clusters just outside the trail in Figure VIII.6.

Based on the hypothetical model for the concentration profile in the wake,

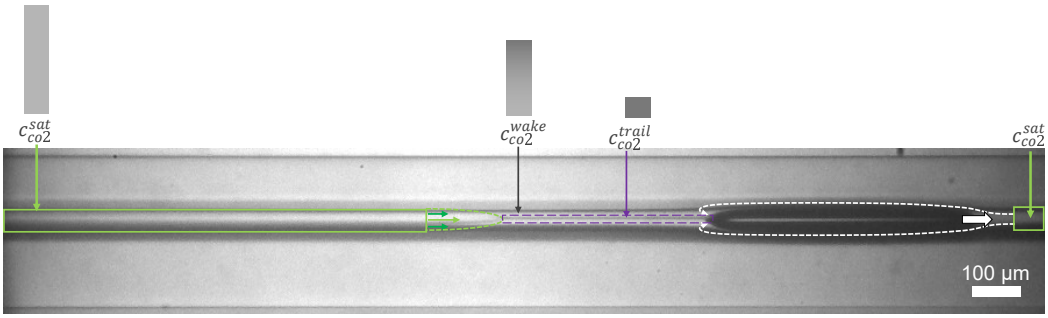

Figure VIII.9: An "anatomy" of the wake left behind an elongated bubble with hypothetical estimations of the relative concentrations of CO_2 in different regions. The bubble (dark object in the inner stream on the right) is moving to the right at a speed faster than the flow. Consequently, the inner stream will end up passing from head to tail of the bubble and filling the space in the back (dashed white arrows), forming a trail in the center of the inner stream (dashed purple box—see Figure VIII.8) with concentration of CO_2 c_{co2}^{trail}. Outside the trail, the concentration of CO_2 c_{co2}^{wake} is higher. Due to the velocity gradient within the inner stream (indicated by green arrows), the interface (green dashed parabola) between the wake and the unperturbed inner stream (outlined in solid green) becomes stretched over time into a parabolic shape. The higher concentration of CO_2 in the unperturbed region of the inner stream c_{co2}^{sat} leads to a difference in index of refraction along this parabolic interface and, therefore, a visible interface. PPG 2700 g/mol polyol (see Table II.1) saturated with CO_2 at 7.2 MPa and 22 °C flowed within sheath of 1k5f polyol in a quartz observation capillary of 300 μm inner diameter and 100 mm length with an inlet pressure of 13.4 MPa and observed at 95 mm along the length of the capillary.

we propose the "anatomy" of the wake shown in Figure VIII.9. In the region of the inner stream in front of the bubble (right side of the image), the concentration of CO_2 is the initial saturation concentration c_{CO2}^{sat}, excepting some depletion along the outside. As the bubble grows, it causes fluid previously near its head to end up at its tail. This fluid forms the wake. At the center of the wake is the trail, which has the lowest concentration of CO_2, c_{CO2}^{trail}. Outside this region, the concentration of CO_2 c_{CO2}^{wake} is greater, but still less than the initial saturation concentration due to depletion of CO_2 through diffusion into the outer stream. While the end of the wake (outlined in a dashed green parabola) begins flat, it becomes stratified due to the velocity gradient with radial distance from the center of the inner stream. Upstream from this interface, the concentration of CO_2 is once again near its saturation concentration c_{CO2}^{sat}.

VIII.3 Ripening and Coalescence

In general, the present thesis focuses on bubbles that grow in isolation so that the growth can be accurately modeled and extrapolated back to the point of nucleation (see Section V.4). Near the outlet of the observation capillary, however, enough bubbles nucleate and grow to a large enough size that they come into contact with each other. As the bubbles continue to grow, the confinement by the outer stream causes them to squeeze against each other. After enough time in close contact, the bubbles merge into one. Minogue recorded merging events in polyurethane foaming experiments (see pp. 130–131 of [5]) that he attributed to ripening in some cases and coalescence in others, but observations were made over the course of several seconds. Is ripening or coalescence dominant in the microfluidic flow-focusing channel?

To answer this question, we show an example of the merging of two bubbles in Figure VIII.10. After nucleating near each other along the trail of the wake of an elongated bubble, the bubbles (outlined by ellipses) squeeze against each other as they grow against the confinement of the outer stream (panel b), ultimately merging into one bubble (panel c). The bubbles merge about 500 μs after coming into contact with each other. Because we could not distinguish how the bubbles merged (ripening: one bubble grows at the expense of the other; coalescence: the liquid film between the bubbles breaks up), we distinguish the two processes by their time scale.

The time scale for ripening of a small bubble into a larger bubble is roughly the time for the fluid inside the smaller bubble to diffuse across the membrane between the bubbles. This time scale τ_{ripen} is therefore proportional to the mass of gas inside the smaller bubble m_1 and inversely proportional to the flux between the bubbles Φ and the area of contact A_c (see diagram in Figure VIII.10d). The mass inside the smaller bubble $m_1 = c_1 V_1$, where c_1 is the concentration of gas in the smaller bubble and V_1 is its volume. The flux of gas between the bubbles scales as the product of the diffusivity $\mathcal{D}$ and the concentration gradient, which can be estimated as the difference in concentrations divided by the thickness of the film between them, which scales as the critical film thickness of rupture h_c since the film thins quickly before reaching this thickness, so $\Phi \sim \mathcal{D}\frac{c_1 - c_2}{h_c}$, where c_2 is the concentration of gas in the larger bubble ($c_2 < c_1$ due to the higher Laplace pressure in the smaller bubble 1). The critical film thickness between two bubbles in contact can be estimated from the work of Frostad *et al.* as $h_c \sim R_1 \bar{F}^{1/6} A^{1/3}$, where $\bar{F}$

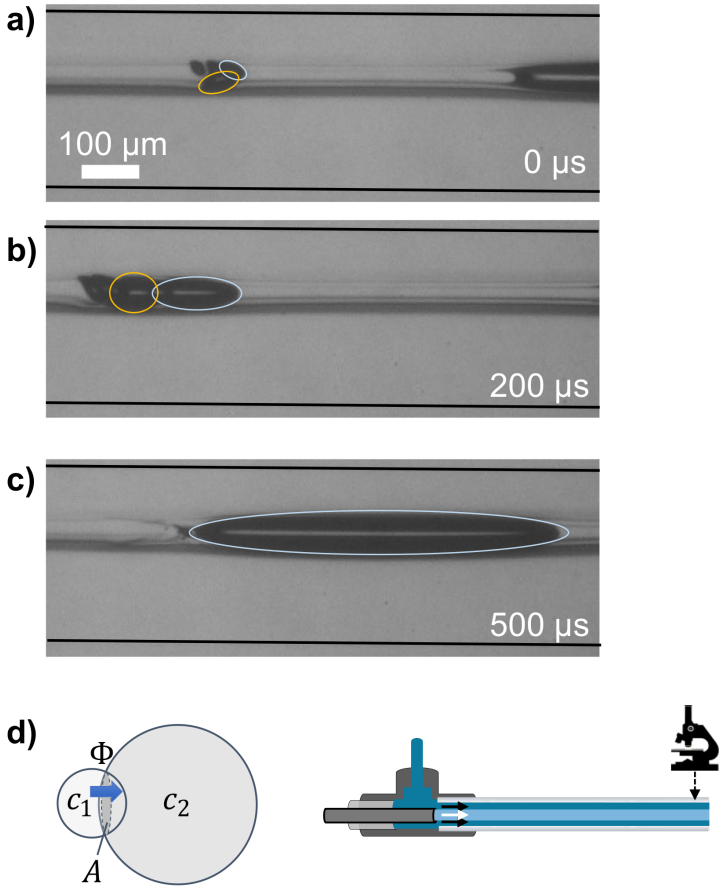

Figure VIII.10: Sequence of images shows two bubbles in contact merge through ripening (a-c). The two bubbles are outlined (orange and blue) until they merge in (c) (blue). d) Schematic of the geometry of two bubbles squeezed against each other. Inner stream of PPG 2700 g/mol saturated with CO_2 at 7.0 MPa and 22 °C was flowed at 50 μL/min in an outer stream of 1k5f polyol (see Table II.1) at 225 μL/min and observed with 4x magnification (see Table III.1) at 94 mm along the observation capillary. The inlet pressure of the observation capillary was 9.5 MPa.

is the force applied on the bubbles F scaled by the interfacial tension σ and the bubble radius R_1, so $\bar{F} = F/(\sigma R_1)$ and A is the dimensionaless Hamaker constant $A = A_H/\sigma R_1^2$, where A_H is the Hamaker constant for the fluid [6]. Finally, the area of contact between the bubbles can be estimated from observation as $A_c = \pi R^2$. Thus, the ripening time scales as $\tau_{ripen} \sim \frac{c_1 R_1^3 h_c}{\mathcal{D}(c_1 - c_2) R_1^2}$. If we assume that the concentrations follow Henry's Law, then, Henry's constant cancels out and the ripening time scale can be written as

$$\tau_{ripen} \sim \frac{p_1 R_1 h_c}{\mathcal{D}(p_1 - p_2)} \tag{VIII.1}$$

where $p_1 = p + 2\sigma/R_1$ and $p_2 = p + 2\sigma/R_2$ are the pressures inside the two bubbles, equal to the local fluid pressure p plus the Laplace pressure.

In the experiment from which the images in Figure VIII.10 were taken, the following estimates were determined for these quantities. We consider the smaller bubble to have a radius between 5 μm and 10 μm while the larger bubble has a radius between 20 μm and 25 μm. The local fluid pressure is estimated as 0.7 MPa assuming a constant pressure gradient along the observation capillary, but it could be as well as 0.3 MPa if the unobservable last 5 mm of the observation capillary are completely filled with bubbles. The interfacial tension under these conditions is between 15 and 25 mN/m (see Figure II.3a). The diffusivity will be governed by the saturation pressure of 7 MPa, so it lies between 5×10^{-10} m^2/s and 1.5×10^{-9} m^2/s. From visual observation, the radius of the area of contact is somewhere between half to the full radius of the inner stream (25 μm), so $R_c \in [12.5, 25]$ μm. The Hamaker constant for glycerol is about twice that of water, which is 3.6×10^{-20} J, so we bound it between $A_H \in [3.6, 7.2] \times 10^{-20}$ J. We estimate the force between the bubbles as the Laplace pressure multiplied by the area of contact $F \sim 2\sigma/R_{bubble} \times R_c^2$. From these ranges, we can estimate the range for the ripening time to be $\tau_{ripen} \in [1, 25]$ ms. The value is slightly larger than observed, but is within the right order of magnitude, as expected for a scaling analysis.

We next compare this time scale with that of coalescence. Frostad *et al.* also estimated the time scale of coalescence and validated their scaling with experiments [6]. For that time scale, they gave the value $\tau_{coalesce} \sim \frac{\eta R}{\sigma} \bar{F}^{1/4} A^{-1/2}$, where η is the viscosity of the fluid and R is the scale for the radius of contact (the first factor is the capillary time). Noting that the estimate for the viscosity of the inner stream lies between 0.01 Pa.s and 0.03 Pa.s, the range for the coalescence time $\tau_{coalesce} \in [30, 2600]$ ms, which is far above the time scale observed. Therefore, between coalescence and ripening, we believe that ripening is the more common merging process at the short time scales over which merging can be observed in this apparatus.

VIII.4 Stream Instabilities

In the present work, the inner stream was kept stable to maintain a consistent environment for bubble nucleation. In some cases, however, the inner stream became unstable. While these instabilities prevented the accurate measurement of bubble nucleation for the purposes of this work, they yielded some fascinating flow patterns

that we discuss in this Section.

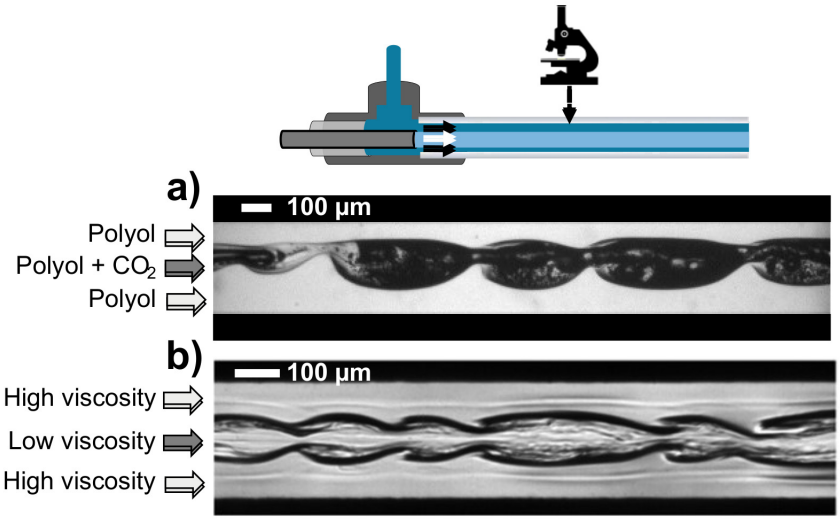

Figure VIII.11: Images of Kelvin–Helmholtz-like instabilities in microfluidic sheath flow. a) 1k3f polyol (see Table II.1) saturated with CO_2 at 8.8 MPa and 22 °C flowed within sheath of 1k5f polyol in quartz observation capillary of 300 μm inner diameter and 100 mm length at 55 mm along the length of the capillary. The opaque regions are bubbles that have nucleated inside the inner stream. Flow enters from the left. b) Low-viscosity (0.49 mPa.s) silicone oil flowing at 900 μL/min in a sheath of high-viscosity (485 mPa.s) silicone oil flowing at 100 μL/min. Adapted from X. Hu and T. Cubaud *Phys. Rev. Fl.* 2016 1:044101 Copyright 2016 American Physical Society.

One common instability was the formation of ligaments and vortices along the inner stream, as shown in Figure VIII.11a. In this experiment, the inner stream was composed of 1k3f polyol (see Table II.1) saturated with CO_2 at 8.8 MPa and 22 °C and the outer stream was 1k5f polyol. In this experiment, the inner stream had a low enough viscosity and a high enough rate of nucleation that nucleation was observed 55 mm along the observation capillary, where the image in Figure VIII.11a was taken, though the inlet pressure was in excess of 15 MPa. While the inner stream never broke up into droplets, as can happen for an immiscible inner stream, its interface developed oscillations and wave-like ligaments that folded in on themselves. The interior of the inner stream flowed much more quickly than these instability patterns at the interface as bubbles jetted along the winding path inside them. Such a pattern was observed in microfluidic sheath flow by Hu and Cubaud when flowing a low-viscosity silicone oil inside a silicone oil of much higher viscosity [7]. The instability is akin to the Kelvin–Helmholtz instability that arises when fluid flows more quickly past another, causing the patterns similar to

the crashing of waves along the interface. Indeed, the speed in the inner stream is significantly higher than that of the outer.

Hu and Cubaud found that the flow is significantly destabilized when the Reynolds number of the inner stream exceeds 90. Despite the small dimensions of the flow and low viscosity of the bubbly flow in the inner stream, such a Reynolds number is plausible given the high speed (several meters per second) and low viscosity of the inner stream apparent from the video. Nevertheless, the Reynolds number can be kept low enough to stabilize the flow by delaying the onset of bubble nucleation in the channel. Bubble nucleation can be delayed by maintaining a high inlet pressure through a high outer stream flow rate, limiting the flow rate of the inner stream, and limiting the saturation pressure of the polyol used for the inner stream. For a thorough depiction and discussion of the stabilization and onset of this instability, see the publication by Hu and Cubaud [7].

When polyol is mixed with cyclopentane the viscosity is lowered significantly due to the low viscosity of cyclopentane (about 0.5 mPa.s at room temperature and pressure [8]), especially after dissolving CO_2. Although the conditions would be suitable for a Kelvin–Helmholtz instability like that shown in Figure VIII.11, when not too many bubbles have nucleated, a different instability pattern emerges, shown in Figure VIII.12. In this experiment, 1k5f polyol (see Table II.1) was mixed with 15% cyclopentane by weight before saturating with CO_2 at 9 MPa. This fluid was flowed through the inner stream at a flow rate more than twice the flow rate of the outer stream of pure 1k5f polyol (70 μL/min vs. 30 μL/min). The fluids flowed through a quartz capillary of 200 μm in inner diameter and 100 mm in length, and were observed at 94 mm along the capillary. Bubbles would appear as opaque, but are not seen in this image, so we assume that bubbles had not yet nucleated despite the high degree of supersaturation, perhaps due to the narrow inner diameter of the observation capillary. Nevertheless, a difference in index of refraction can be distinguished, which reveals periodically spaced vortex-like patterns connected by what appear to be interwoven threads of fluid. We have not found such a flow instability in the literature, although the pearl and mushroom instability reported by d'Olce *et al.* is similar [9].

References

1. Revellin, R., Agostini, B. & Thome, J. R. Elongated bubbles in microchannels. Part II: Experimental study and modeling of bubble collisions. *International Journal of Multiphase Flow* **34,** 602–613. ISSN: 03019322 (2008).

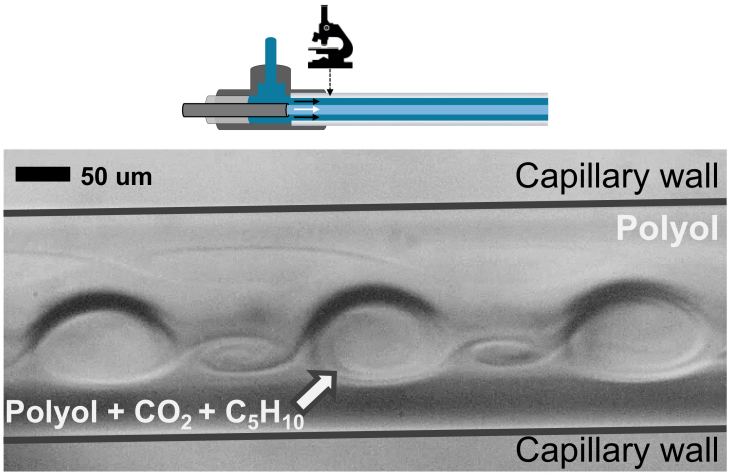

Figure VIII.12: Instability within inner stream of 1k5f polyol (see Table II.1) mixed with 15% cyclopentane by weight and saturated with CO_2 at 9 MPa flowed at 70 μL/min within a sheath of 1k5f polyol at 30 μL/min. The fluids flowed through a quartz capillary of 200 μm in inner diameter and 100 mm in length, and were observed at 20 mm along the capillary. Evenly spaced vortices appear to be linked by interwoven threads of fluid.

2. Agostini, B., Revellin, R. & Thome, J. R. Elongated bubbles in microchannels. Part I: Experimental study and modeling of elongated bubble velocity. *International Journal of Multiphase Flow* **34,** 590–601. ISSN: 03019322 (2008).

3. Yin, L., Jia, L., Guan, P. & Liu, D. Experimental investigation on bubble confinement and elongation in microchannel flow boiling. *Experimental Thermal and Fluid Science* **54,** 290–296. ISSN: 08941777. http://dx.doi.org/10.1016/j.expthermflusci.2014.01.004 (2014).

4. Khandekar, S., Panigrahi, P. K., Lefèvre, F. & Bonjour, J. Local Hydrodynamics of Flow in a Pulsating Heat Pipe: A Review. *Frontiers in Heat Pipes* **1.** ISSN: 2155-658X. https://www.thermalfluidscentral.org/e-journals/index.php/Heat_Pipes/article/view/103 (Nov. 2010).

5. Minogue, E. *An in-situ study of the nucleation process of polyurethane rigid foam formation* PhD thesis (Dublin City University, 2000), 1–194. http://doras.dcu.ie/19076/.

6. Frostad, J. M., Paul, A. & Leal, L. G. Coalescence of droplets due to a constant force interaction in a quiescent viscous fluid. *Physical Review Fluids* **1,** 1–14 (2016).

7. Hu, X. & Cubaud, T. Inertial destabilization of highly viscous microfluidic stratifications. *Physical Review Fluids* **1,** 044101. ISSN: 2469990X (2016).

8. Kurihara, K., Kandil, M. E., Marsh, K. N. & Goodwin, A. R. H. Measurement of the Viscosity of Liquid Cyclopentane Obtained with a Vibrating Wire Viscometer at Temperatures between (273 and 353) K and Pressures below 45

MPa. *Journal of Chemical & Engineering Data* **52,** 803–807. ISSN: 0021-9568. https://pubs.acs.org/doi/10.1021/je060416d (May 2007).

9. D'Olce, M., Martin, J., Rakotomalala, N., Salin, D. & Talon, L. Pearl and mushroom instability patterns in two miscible fluids' core annular flows. *Physics of Fluids* **20,** 024104. ISSN: 10706631 (2008).

VIII.S1 Stagnation of Bubbles

In the main text, small bubbles were seen to stagnate when an elongated bubble passed by them (Figure VIII.3). In Figure VIII.S1, we show that even bubbles in the outer stream slow down as elongated bubbles pass by. The reduction in speed caused by the passing of an elongated bubble is smaller in the outer stream than the inner stream due to the slower initial speed in the outer stream than the inner stream, so the effect is less obvious here. This slow-down indicates that the transport of fluid from the head to the tail of an elongated bubble occurs not just in the inner stream, but in the outer stream as well. It also shows that the significant reduction in the pressure drop along an elongated bubble is quickly felt throughout the inner and outer streams.

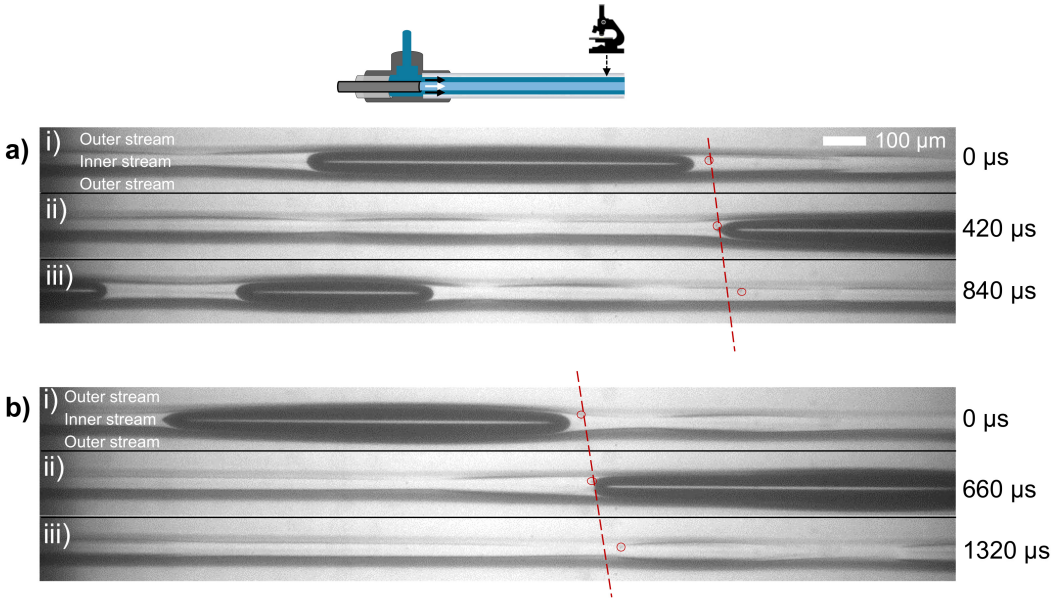

Figure VIII.S1: Still frames show how two small bubbles in the outer stream (circled in red) slow down almost to stagnation when an elongated bubble passes by them. In the top two frames of (a) and (b), the bubble in the outer stream moves minimally as an elongated bubble passes it. From the second to the third frame, the same time passes, but the bubble travels a farther distance, indicating that the passage of the elongated bubble slowed the flow even in the outer stream (although not to a complete stop). This difference in speed is demonstrated by the deviation from the extrapolation of the speed marked by the red dashed lines. Note that we determined that the bubble is in the outer stream due to its significantly slower speed and lack of growth.

VIII.S2 Nucleation of Bubbles in the Wake of an Elongated Bubble

In Figure VIII.S2, we show the nucleation of bubbles along the trail in the wake of an elongated bubble, followed by their growth, ripening, merging into a larger, elongated bubble, and subsequent nucleation of bubbles in the wake once again. The bubbles in the wake nucleate along the trail left behind the elongated bubble, which we suggest is the remnant of the depletion boundary layer formed as the bubble passed along the inner stream fluid (see Figure VIII.8). Bubbles likely nucleate around the same time due to a sudden decrease in the local pressure as a larger bubble reached the end of the observation capillary. The bubbles likely ripen instead of coalescing based on the time scale of merging (see discussion in Section VIII.3). This cycle may repeat many times as elongated bubbles exit the observation capillary and cause sudden decreases in pressure. These decreases in pressure are only significant near the end of the observation capillary where the pressure is on the order of atmospheric pressure.

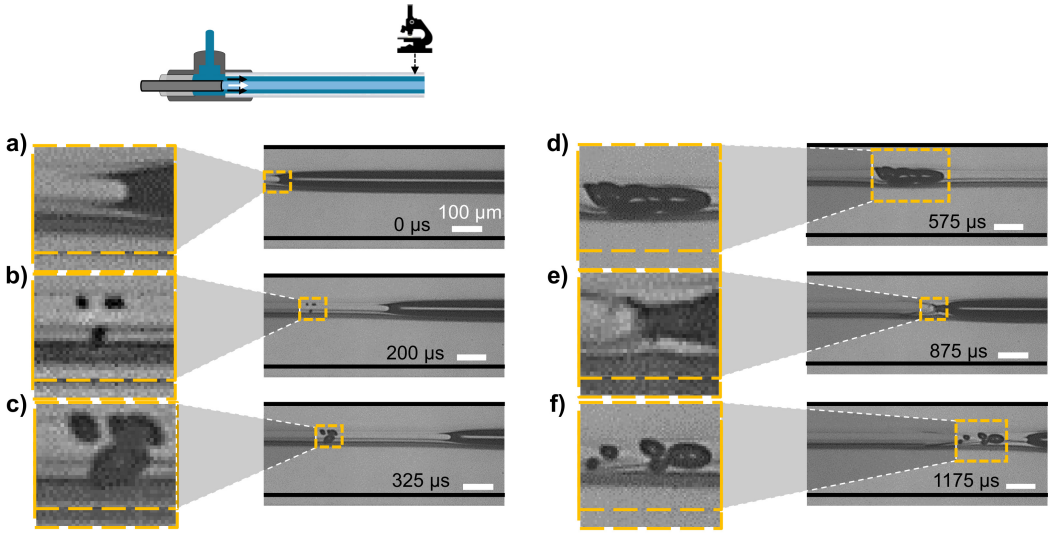

Figure VIII.S2: Depiction of bubble nucleation in the wake of an elongated bubble followed by merging and more nucleation in the wake. Images are zoomed in the panels on their left. Times from the first frame are recorded at the bottom. a) A wake is observed at the tail of an elongated bubble. b) Bubbles nucleate just outside the trail left in the wake of the elongated bubble, consistent with the schematic picture presented in Figures VIII.6 and VIII.8. c) The just-nucleated bubbles grow and come into contact with each other. d) The bubbles grow more and squeeze against each other, causing them to extend along the inner stream. e) The bubbles merge through ripening (see discussion in Section VIII.3) into another elongated bubble. f) The newly formed elongated bubble causes nucleation in its wake. This cycle repeats until CO_2 is depleted sufficiently in the wake.